applied sciences

MDPI

Article

Effect of OSEM Reconstruction Iteration Number and Monte Carlo Collimator Modeling on ^{166}Ho Activity Quantification in SPECT/CT

Rita Albergueiro [1,2,3,*], Vera Antunes [2] and João Santos [1,2,4,5]

[1] Department of Physics and Astronomy, Faculty of Sciences of University of Porto (FCUP), Rua do Campo Alegre 1021 1055, 4169-007 Porto, Portugal; joao.santos@ipoporto.min-saude.pt
[2] Medical Physics, Radiobiology and Radiation Protection Group, IPO Porto Research Center, Portuguese Oncology Institute of Porto, Rua Dr. António Bernardino de Almeida, 4200-072 Porto, Portugal; vera.antunes@ipoporto.min-saude.pt
[3] Department of Nuclear Medicine, São João University Hospital Center, Alameda Prof. Hernâni Monteiro, 4200-319 Porto, Portugal
[4] Department of Nuclear Medicine, Santo António University Hospital Center, Largo Prof. Abel Salazar, 4099-001 Porto, Portugal
[5] Instituto de Ciências Biomédicas Abel Salazar (ICBAS), Rua de Jorge Viterbo Ferreira 228, 4050-313 Porto, Portugal
* Correspondence: ritaalbergueiro@gmail.com

Abstract: Background: Accurate reconstruction and quantification in the post-therapy SPECT/CT imaging of ^{166}Ho microspheres for hepatic malignancies is crucial for treatment evaluation. This present study aimed to explore the impact of the OSEM reconstruction parameters on SPECT/CT image features for dose distribution determination, using Hybrid Recon™ (Hermes Medical Solutions AB) and full Monte Carlo (MC) collimator modeling. Methods: Image quality and activity quantification were assessed through two acquisitions of the Jaszczak phantom using a Siemens Symbia Intevo Bold SPECT/CT system. The datasets were reconstructed using the OSEM method, with variations in the number of iterations for 15 and 8 subsets, both with and without full MC collimator modeling. Contrast recovery coefficient (Q_H), coefficient of variation (CV), contrast-to-noise ratio (CNR), calibration factor (CF), and activity recovery coefficient (ARC) were calculated and used to evaluate image quality and activity quantification. Results: Reconstructions with 5 iterations and 15 subsets, as well as 10 iterations and 8 subsets, were selected as the most suitable for ^{166}Ho imaging, as they provided higher Q_H and ARCs. Incorporating full MC collimator modeling in both reconstructions led to significant improvements in image quality and activity recovery. The CFs remained consistent for a fixed value of 15 and 8 subsets, with values of (14.9 ± 0.5) cps/MBq and (14.6 ± 0.5) cps/MBq, respectively. However, when applying full collimator modeling, the CF values decreased to a range between 10.9 and 12.1 cps/MBq. Conclusions: For ^{166}Ho SPECT/CT imaging, OSEM (with either 5 iterations and 15 subsets or 10 iterations and 8 subsets) combined with full MC collimator modeling yielded superior image quality and quantification results.

Keywords: ^{166}Ho; radioembolization; SPECT/CT reconstruction; SPECT/CT quantification; image quality

check for updates

Academic Editor: Thomas Lindner

Received: 16 November 2024
Revised: 27 January 2025
Accepted: 3 February 2025
Published: 5 February 2025

Citation: Albergueiro, R.; Antunes, V.; Santos, J. Effect of OSEM Reconstruction Iteration Number and Monte Carlo Collimator Modeling on ^{166}Ho Activity Quantification in SPECT/CT. *Appl. Sci.* **2025**, *15*, 1589. https://doi.org/10.3390/app15031589

Copyright: © 2025 by the authors. Licensee MDPI, Basel, Switzerland. This article is an open access article distributed under the terms and conditions of the Creative Commons Attribution (CC BY) license (https://creativecommons.org/licenses/by/4.0/).

1. Introduction

In the treatment of primary and secondary liver cancer, radioembolization with holmium-166 microspheres (^{166}Ho-RE), also known as SIRT (Selective Internal Radiation

Therapy), appears as a promising therapy. This procedure, as in other liver radioembolization techniques (^{90}Y-based), involves injecting radioactive microspheres into the hepatic artery through a microcatheter placed in the femoral artery [1].

A small activity of ^{166}Ho microspheres, typically 200-250MBq, serves as a "scout dose" to assess the microspheres' distribution within the liver and detect any extra-hepatic shunting. This is achieved through a post-scout SPECT/CT scan, which guides the planning and administration of the main treatment involving a higher activity of ^{166}Ho microspheres. After this verification and planning first step, a therapeutic activity of typically 2-6 GBq is injected, mimicking the "scout dose" distribution.

After administering the therapeutic activity, a post-therapy SPECT/CT scan is performed after a suitable interval of time has elapsed. This delay ensures that the SPECT detectors are not saturated by the high count rate immediately following the treatment due mainly to Bremsstrahlung radiation emission [2]. The second SPECT scan enables the assessment of the doses delivered to both the liver and the tumor.

^{166}Ho is a high-energy beta-emitting radioactive isotope (maximum energy: 1.85 MeV, abundance 49%). It also emits low-energy gamma rays at 80.6 keV (abundance 6.6%), which enables the visualization of microspheres' distribution through SPECT (Single-Photon Emission Computed Tomography) [1,3,4]. Additionally, there are gamma emissions at higher energies, including 1.34 MeV (0.9%), 1.58 MeV (0.2%), and 1.66 MeV (0.1%) [5].

When working with ^{166}Ho, it is crucial to account for the presence of Bremsstrahlung radiation and Compton scattering. The high-energy photons in the Bremsstrahlung spectrum can pass through the collimator septa, leading to a reduced image quality and causing inaccurate results [6].

MC algorithms that simulate scattering within the object have been effective in recovering image information. The Hybrid Recon™ software by Hermes Medical Solutions AB (Stockholm, Sweden) incorporates a scatter modeling method named "convolution-based forced detection", applying pre-calculated probability density functions of the ^{166}Ho spectrum generated using the PENELOPE MC code [7,8].

This approach by Hybrid Recon™ includes a full MC collimator simulation, which comprehensively addresses all photon interactions at the collimator, including both primary and scattered photons, while also considering scatter within the object [8].

As the interest in post-therapy dosimetry grows [9], accurate quantification of ^{166}Ho becomes necessary. Thus, properly determining the CF, which is required to convert SPECT image counts into radioactivity concentration units (MBq/mL), plays a critical role in activity quantification [10,11]. It is important to note that radioembolization enables direct activity conversion from SPECT scans, as nearly all activity stays within the liver, removing the need for a calibration factor.

It is also essential to address the PVE when discussing ^{166}Ho activity quantification. PVE is an important factor that affects the measurement of activity concentration in emission tomographic imaging and can significantly impact the accuracy of radionuclide uptake determination in quantitative SPECT and PET imaging. To address this issue and potentially correct it, one approach is to use ARC along with the corresponding activity concentration recovery curves [12].

The primary goal was to enhance the OSEM reconstruction parameters (number of iterations and subsets) for ^{166}Ho SPECT and assess the impact of advanced MC collimator modeling through Hybrid Recon™ on both image quality and quantification. The secondary objectives were to calculate the CF for ^{166}Ho SPECT/CT, assess the impact of reconstruction parameters on the CF, and determine the ARC as a function of sphere volume.

2. Materials and Methods

2.1. SPECT/CT Imaging Protocol

Images were acquired in a Siemens Symbia Intevo Bold SPECT/CT.

The imaging parameters were set as follows: a non-circular step-and-shoot 360° orbit with 60 views per head and each view lasting 20 s. A matrix size of 128 × 128 and a pixel size of 4.8 mm were used for SPECT data acquisition.

The photopeak energy window was set at 80.6 keV with a width of 15%. A scatter energy window centered at 118 keV with a width of 12% was utilized to account for scatter from higher-energy gamma emissions and Bremsstrahlung [2].

CT scans were performed prior to SPECT acquisition using a tube voltage of 110 kVp and a tube current–time product of 40 mAs.

To minimize the impact of Bremsstrahlung radiation and high-energy gamma rays emitted by ^{166}Ho, medium-energy low-penetration (MELP) collimators were employed for all SPECT/CT acquisitions.

2.2. Phantom Acquisitions

A Jaszczak phantom was used to assess the quality of the reconstructed images, to perform activity quantification, and, thus, to determine the CF. The phantom spheres had diameters ranging from 6.23 mm to 31.27 mm [13] and were filled with a 2.51 MBq/mL ^{166}Ho chloride solution. The background compartment of the phantom contained only water and no activity. Subsequently, SPECT/CT data were collected (Figure 1B).

A second acquisition was carried out with activity in the background and a sphere-to-background ratio of 30:1 (Figure 1C), resulting in a background concentration of 0.074 MBq/mL.

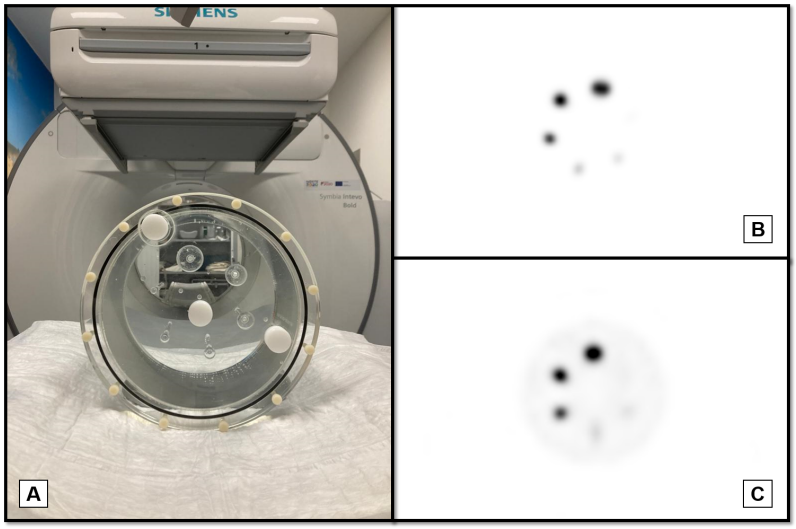


Figure 1. SPECT/CT images of the Jaszczak phantom. (**A**) Phantom setup for acquisition; (**B**) SPECT transaxial slice without background activity; (**C**) SPECT transaxial slice with background activity.

2.3. SPECT/CT Reconstructions

The reconstructions of the SPECT/CT datasets used the OSEM method, which is one of the available techniques in the Hybrid Recon™ 4.0 software.

Multiple reconstructions of the phantom SPECT/CT data were performed, varying the number of iterations from 1 to 7 while keeping constant 15 subsets, which is the default value in Hermes. The same protocol was employed in [8] for a ^{90}Y study. Additionally, the impact of varying the number of iterations from 1 to 14 with a 8 fixed subsets was also investigated. The reconstruction process involved applying a FWHM of 0.9 cm and

incorporating all available corrections in the Hybrid Recon™ software (motion, attenuation, and scatter corrections).

Attenuation correction using the CT data was performed and the resolution recovery option was enabled. Furthermore, standard MC scatter correction was applied to enhance the quality of the reconstructed images.

For all these reconstructions, the ones providing the best combination of image quality and activity quantification were identified, as described below. The selected reconstructions were then reprocessed with full MC collimator modeling, and a comparison between them was performed.

2.3.1. Image Quality

Image contrast and noise were calculated for each reconstruction relative to the second phantom acquisition to assess the impact of the number of iterations on image quality. By analyzing these values and identifying the reconstructions that yielded the highest Q_H and lowest noise, the study aimed to determine if an optimal number of iterations could be established.

Spherical volumes of interest (VOIs) corresponding to the hot spheres were delineated on the CT images using Hybrid Viewer™ (Hermes Medical Solutions AB). The VOIs were created with inner diameters matching those of the hot spheres. Similarly, VOIs of the same diameter were drawn concentrically in three different regions of the background: above, beside, and below the sphere, following the approach adapted from [8]. The VOIs were then copied onto the corresponding aligned SPECT image. For each one of the six hot sphere VOIs, the Q_H was calculated using the following equation [14]:

$$Q_H = \frac{\frac{C_H}{C_B} - 1}{R - 1} \times 100\% \quad (1)$$

C_H represents the average counts within the hot sphere VOI, C_B represents the average of the mean counts in the three background VOIs, and R represents the ratio of the activity concentration between the hot spheres and the background.

The CV was used as a measure of image noise, calculated using Equation (2) [14]. $STDV_B$ represents the standard deviation of all voxels within the background VOI, which was specifically delineated in a region with minimal influence from the hot spheres, containing only background activity. The CV was calculated for each reconstruction performed.

$$CV = \frac{STDV_B}{C_B} \times 100\% \quad (2)$$

As a final image quality measure, the contrast-to-noise ratio (CNR) was calculated for the reconstructions selected as the most suitable using Equation (3) [15]. This metric was used to assess object detectability based on the Rose criterion (CNR > 5) [15,16].

$$CNR = \frac{C_H - C_B}{STDV_B} \quad (3)$$

2.3.2. Activity Quantification

The calibration factors were obtained using the second phantoms acquisitions (with background activity). It was assumed that the region below the hot spheres region, which was uniformly filled with ^{166}Ho, was not influenced by the spheres themselves.

Using Hybrid Viewer™, a total of 20 spherical VOIs were delineated in the background compartment. These VOIs were selected to have the same volume. The count rate within each VOI (C_{VOI_i}) was recorded. The activity in each VOI (A_{VOI}) was calculated by

multiplying the activity concentration of the background compartment by the volume of the respective VOI. After applying Equation (4), the CF was calculated as a function of the iteration number for all reconstructions, also accounting for the influence of MC full collimator modeling. Alongside the CF, the associated uncertainty was also calculated, following the guidelines outlined in [17].

$$\mathrm{CF} = \frac{\sum_{i=1}^{N} \mathrm{C}_{\mathrm{VOI}_i}}{N \cdot A_{\mathrm{VOI}}} \tag{4}$$

ARC as a function of sphere volume was determined using the first set of phantom acquisitions. An ARC for each insert was then determined using two different methods.

In the first method, spherical VOIs matching the size of the physical insert were delineated on the CT scan and then copied into the corresponding SPECT image. The ARC for each sphere was calculated using Equation (5) (adapted from [14]).

$$\mathrm{ARC}_i = \frac{C_i}{\mathrm{CF} \cdot A_i} \tag{5}$$

Considering Equation (5), C_i is the total count rate within each VOI corresponding to insert i, CF is the calibration factor of the respective reconstruction, and A_i is the known activity in insert i (product of activity concentration of the spherical inserts and the volume of the respective insert).

The second method used to determine the ARC followed the EANM (European Association of Nuclear Medicine) guidelines for uncertainty analysis [17]. Using Equation (6), it is the quotient between the observed count rate measured within the insert VOI, denoted as C_i, and the count rate of all counts originating from an oversized VOI that encompass the sphere, denoted as $\mathrm{C}_{\mathrm{total}}$.

$$\mathrm{ARC}_i = \frac{C_i}{C_{total}} \times 100\% \tag{6}$$

Finally, for each method, the ARC data fit was determined using the expression proposed by [17] and expressed through the following equation:

$$\mathrm{ARC}(v) = 1 - \frac{1}{1 + \left(\frac{v}{b}\right)^a} \tag{7}$$

3. Results

Figure 2 shows the $\mathrm{Q_H}$ values obtained for each reconstruction with a fixed number of 15 and 8 subsets, respectively, illustrating their relationship with the number of iterations. The coefficient of variation was also calculated as an indicator of image noise and is presented in Figure 3.

Upon observing Figure 2, a clear difference becomes evident between the three smaller spheres and the three larger spheres. The contrast recovery coefficients for the smaller spheres are below 10%, whereas those for the larger spheres attain higher values up to 50%.

As expected, noise increases with the number of iterations for both sets of data points. It was also observed that when using 8 subsets, the CV up to the 10th iteration still resulted in an image with less noise than the final reconstruction with 15 subsets.

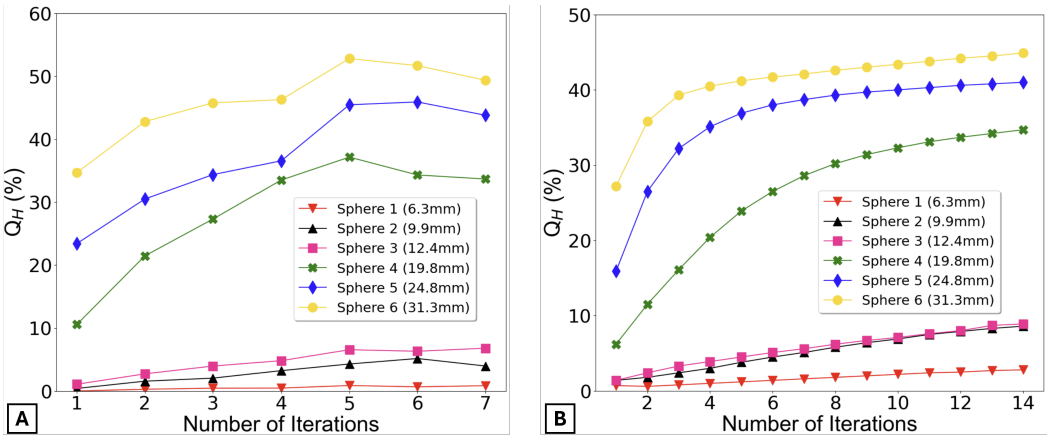


Figure 2. Relationship between the contrast recovery coefficients and the number of iterations for all six spheres. Graph (**A**) shows data for a fixed value of 15 subsets, while Graph (**B**) shows data for a fixed value of 8 subsets.

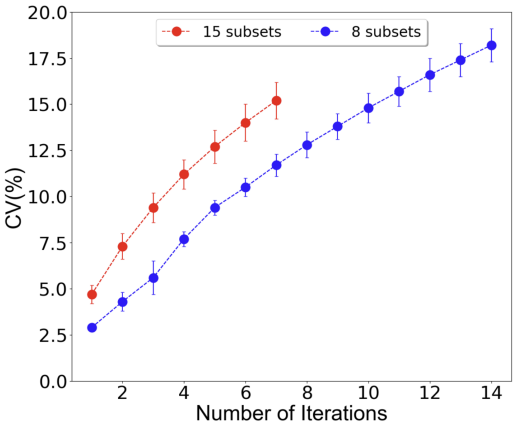


Figure 3. Coefficient of variation (%) as a function of the number of iterations for both fixed subset values.

Figure 4 demonstrates visually the impact of the number of iterations for both fixed subset values.

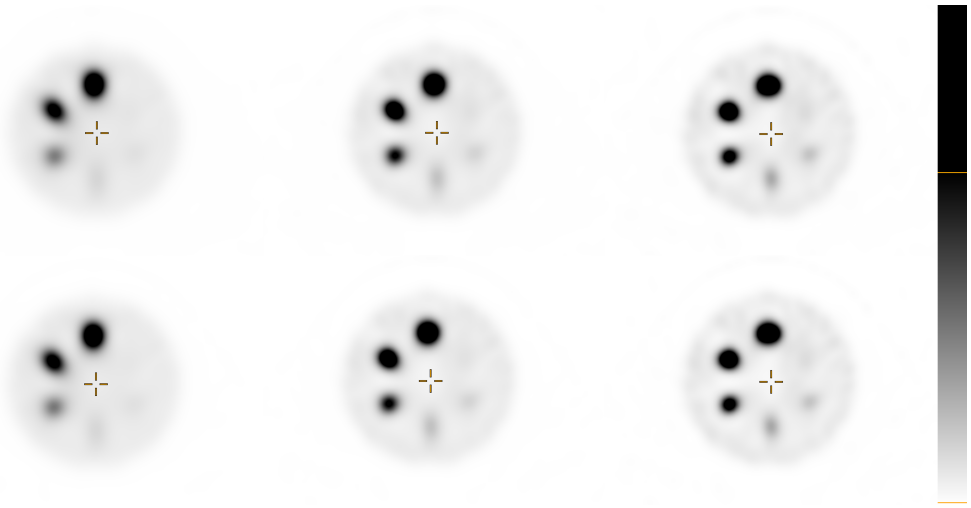


Figure 4. Phantom's reconstructions: 1, 3, and 7 iterations with 15 subsets (**top** row) and 2, 6, and 14 iterations with 8 subsets (**bottom** row).

Both rows display very similar images, as expected, given that the number of iterations in the second row is doubled while the number of subsets is nearly halved compared to the

top row. As anticipated, an increasing number of iterations results in images with a higher contrast and increased noise.

In terms of activity quantification, the CF and its associated uncertainty are shown for each reconstruction in Figure 5, including reconstructions with the same parameters and full MC collimator modeling. Due to the extensive computation time required (which was not feasible with the GPU) and the predictable nature of the results, CF values were only obtained for 1 and 10 iterations, with a fixed number of 8 subsets.

The CFs remain relatively constant with the number of iterations for each subset configuration, with slightly lower values observed for 8 subsets (mean: 14.6 ± 0.5 cps/MBq) compared to 15 subsets (mean: 14.9 ± 0.5 cps/MBq). Additionally, it was observed that applying full MC collimator modeling reduced the CF to values ranging between 10.9 and 12.1 cps/MBq.

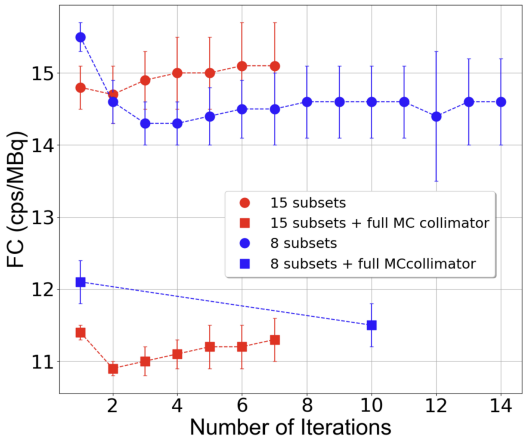


Figure 5. CF (cps/MBq) as a function of the number of iterations for both fixed subset values and including full MC collimator modeling.

The ARCs were determined using two distinct methods. Figure 6 presents the ARC as a function of the number of iterations, calculated using the first method.

By observing Figure 6, it can be said that the ARCs remain practically constant for all spheres after 5 iterations for 15 subsets (graph A) and 10 iterations for 8 subsets (graph B).

After carefully analyzing the contrast, noise, and activity recovery results for all reconstructions, two different reconstructions were selected for further investigation to assess the impact of full MC collimator modeling on the results. The selected reconstructions were as follows: 5 iterations with 15 subsets and 10 iterations with 8 subsets.

Figure 7 visually demonstrates the impact of full MC collimator modeling, along with a profile of the line present in the images, as the differences in the images are not perceptible to the eye.

Figure 8 presents the contrast recovery coefficients and the contrast-to-noise ratio for the final four selected reconstructions. Graph A shows that for the three smaller spheres, the contrast is very similar across all four reconstructions. However, for the three larger spheres, the reconstruction with 10 iterations, 8 subsets, and full MC collimator modeling provides the highest contrast. Graph B shows that the CNR was higher for the reconstruction with 5 iterations, 15 subsets, and full MC collimator modeling.

It is also important to note that none of the reconstructions provided a CNR greater than 5 for the smaller sphere, meaning that this sphere was not detectable in any of the images.

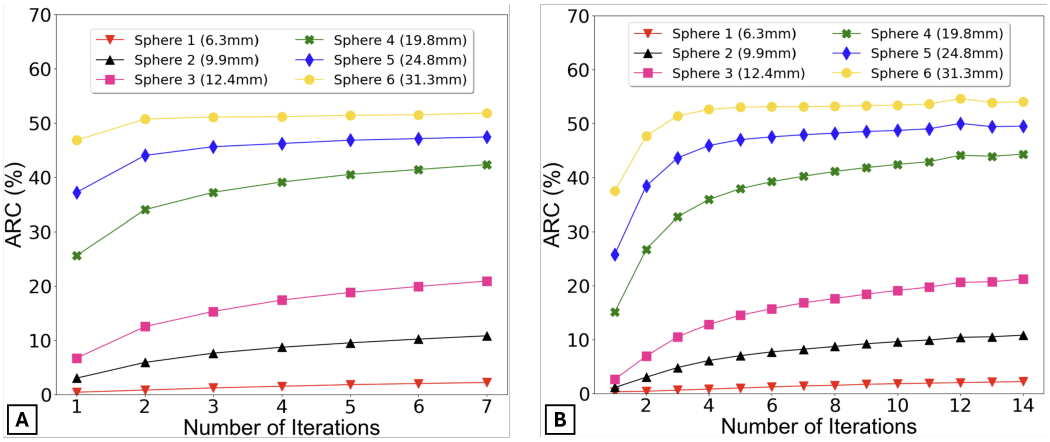


Figure 6. Relationship between activity recovery coefficients and the number of iterations for all six spheres. Graph (**A**) shows data for a fixed value of 15 subsets, while Graph (**B**) shows data for a fixed value of 8 subsets.

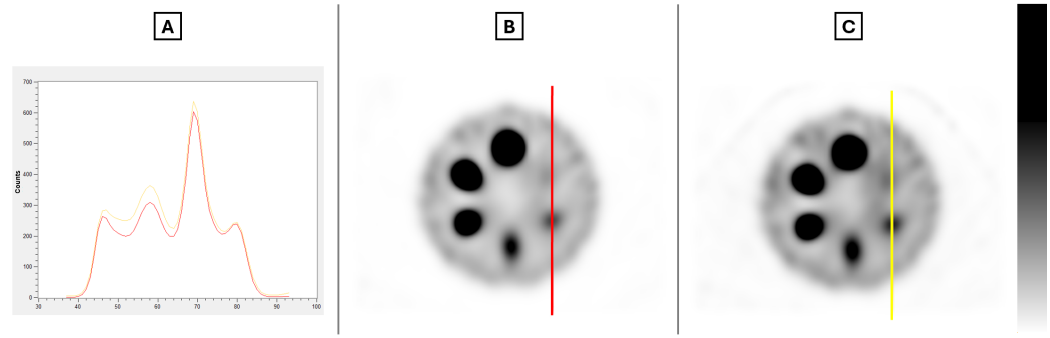


Figure 7. (**A**) Profile in red and yellow lines; (**B**) Phantom's reconstruction of 5 iterations and 15 subsets; (**C**) Phantom's reconstruction of 10 iterations and 8 subsets.

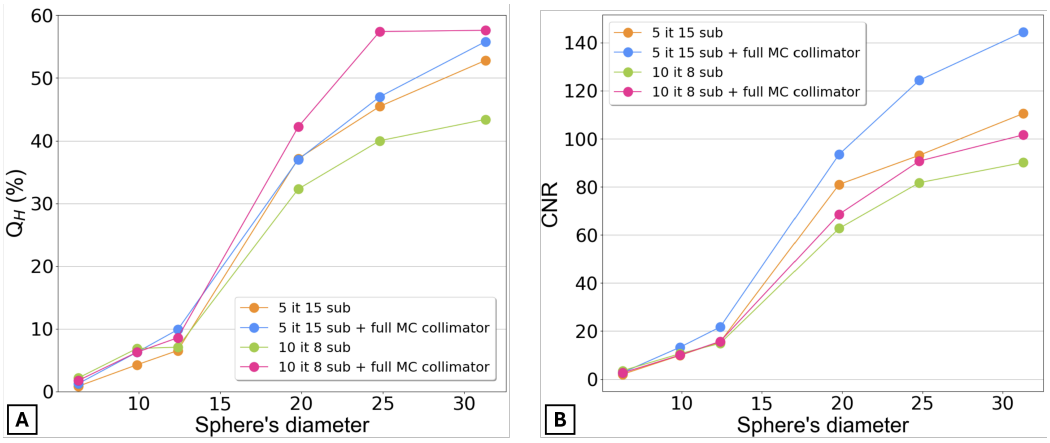


Figure 8. Contrast recovery coefficients (graph **A**) and contrast-to-noise ratio (graph **B**) as a function of the sphere's diameter for the selected reconstructions.

As a final result, Figure 9 displays the ARCs as a function of the sphere's volume for both methods (Equations (5) and (6)). For both graphs, Equation (7) was fitted to the data points, and the determination coefficients (R^2) are shown.

Graph A clearly demonstrates that the reconstruction with 10 iterations, 8 subsets, and full MC collimator modeling provides the highest activity recovery. However, Graph B, which uses the EANM guidelines to calculate the ARC, shows that, regardless of the reconstruction, the ARCs are similar across all reconstructions.

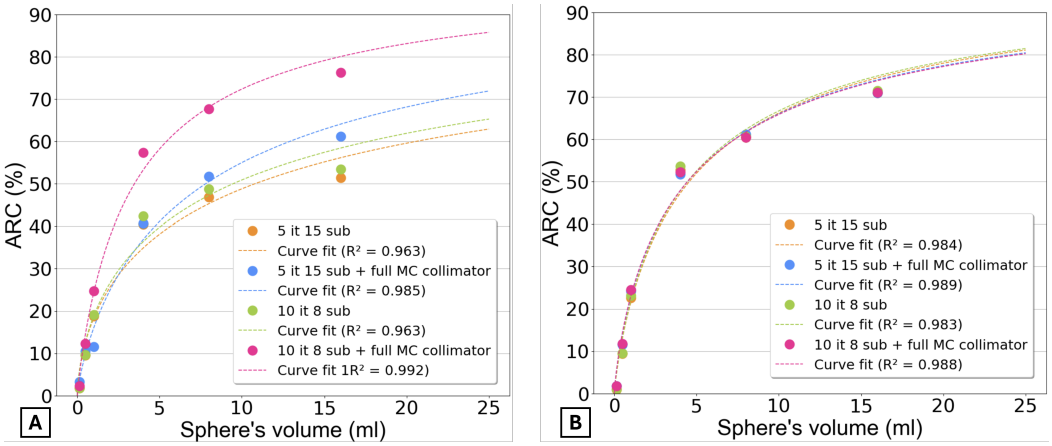


Figure 9. Activity recovery coefficients as a function of the sphere's volume for the selected reconstructions calculated using both methods (graph **A**—first method and graph **B**—second method).

4. Discussion

The aim of the presented data on post-SIRT ^{166}Ho SPECT/CT imaging was to examine the impact of OSEM reconstruction parameters and investigate the advantages of full MC collimator modeling in improving image quality and quantification.

The number of iterations used in the OSEM method can impact the qualitative accuracy of the reconstructed images. However, it is important to highlight that as the number of iterations increases, so does the background noise in the images. This may complicate the visual analysis of images, particularly in detecting small lesions. To address this, the study investigated how varying the number of iterations from 1 to 7 while keeping as constant 15 subsets, as well as varying the number of iterations from 1 to 14 with 8 fixed subsets, would affect the Q_H and noise values.

By analyzing Figure 2A, it is possible to verify that Q_H increases with the number of iterations for all spheres (except the smallest one). However, beyond 5 iterations, the contrast coefficients remain relatively constant, showing no significant increase.

When evaluating Figure 2B, a distinct behavior is observed. The contrast recovery coefficients increase significantly during the initial iterations and then stabilize for the larger spheres. However, for the smaller spheres, Q_H continues to increase linearly.

It was also evident that the coefficient of variation increased correspondingly with the augmented number of iterations in each reconstruction (Figure 3). This outcome aligns with expectations based on the functioning of the OSEM method, where a higher number of iterations corresponds to increased background noise in the resultant images.

As expected, it was also observed in Figure 3 that an increase in the number of subsets corresponded to a rise in CV values for both datasets.

By increasing the number of subsets, the projection data are partitioned into smaller segments. This acceleration in segmentation leads to quicker image updates within each iteration, as each subset contributes insights into a smaller region of the image. However, this accelerated updating process can intensify the reconstruction susceptibility to variations present in the input data [18]. Consequently, the reconstructed image can manifest increased noise, ultimately resulting in a heightened CV, as was observed in these datasets.

Regarding the quantification of ^{166}Ho activity, the study successfully determined the CF for each reconstruction. For each subset value investigated, the CF values were closely aligned, providing a measure of confidence in their consistency. However, when full MC collimator modeling was applied, the CF values were slightly lower. This difference is significant and must be considered to ensure the accuracy and reliability of the CF, confirming its suitability for absolute activity quantification in ^{166}Ho microsphere SPECT/CT imaging.

Additionally, Figure 6 also verifies that the activity recovery stabilizes rapidly with fewer iterations.

After evaluating image quality and activity quantification, the most suitable OSEM reconstruction parameters were determined based on contrast recovery and activity recovery coefficients. For 15 subsets, 5 iterations provided an optimal balance between noise reduction and accuracy. Increasing iterations to 6 or 7 did not improve contrast but increased noise, making additional iterations unnecessary. Among all reconstructions, 5 iterations with 15 subsets yielded the highest Q_H.

Additionally, the reconstruction with 10 iterations and 8 subsets was selected for further analysis, as it achieved high ARC values while maintaining noise levels comparable to the other selected reconstruction.

After identifying the most suitable reconstructions, further investigation was conducted on these two reconstructions and two additional ones with the same parameters but incorporating full MC collimator modeling. Figures 8 and 9A demonstrate that the inclusion of full MC collimator modeling enhances the values of both Q_H and ARC.

A significant challenge in ^{166}Ho SPECT/CT image acquisition arises from the limitations of conventional scatter correction techniques, which are optimized for discrete energy spectra. This issue is particularly notable due to the continuous Bremsstrahlung spectrum of ^{166}Ho. The use of Hybrid Recon™, which incorporates scatter modeling within the detector and collimator, represents a valuable advancement in improving the quantification of ^{166}Ho images, as verified in this study.

However, despite the improved results achieved with full MC collimator modeling, a significant limitation is the extended computation time (processor used: 12th Gen Intel® Core™ i7-12700K; no GPU acceleration supported by the MC algorithm), which is often impractical in clinical settings. For instance, reconstructing 5 iterations with 15 subsets required approximately 2 h, while reconstructing 10 iterations with 8 subsets took nearly 5 h when full MC collimator modeling was applied.

Therefore, using 5 iterations with 15 subsets or 10 iterations with 8 subsets without incorporating full MC collimator modeling remains a highly suitable and practical choice for patient data.

Finally, as observed in Figure 9A, Equation (7) provides a satisfactory fit for the data from both methods. However, it generally aligns better with the second method, which is expected since Equation (7), as proposed by [17], was specifically designed for determining ARC values using the second method.

Additionally, Figure 9A highlights a clear limitation of using only spheres with diameters up to 31 mm, as the recovery curve fails to reach a plateau. This limitation should be considered in future studies as larger-diameter spheres become available.

In summary, multiple methods for determining ARC values are available. The appropriate approach to performing PVE correction on small volumes depends on their specific usage context and the type of SPECT/CT reconstruction applied. Another significant insight from the ARC values analysis was the substantial potential underestimation of activity in small volumes caused by PVE. This highlights the critical need to account for and rectify PVE in local absorbed dose calculations.

5. Conclusions

A detailed analysis of image quality and activity recovery led to the selection of two reconstructions as the most suitable for ^{166}Ho SPECT imaging: 5 iterations with 15 subsets and 10 iterations with 8 subsets. It was found that applying full MC collimator modeling significantly improved both contrast and activity recovery coefficients in these reconstructions. However, the extensive computation time required for these images

presents a major limitation for their practical use in clinical settings. Another important conclusion relates to the CF and how its value changes with different reconstruction parameters. It was observed that applying full MC collimator modeling resulted in lower CF values, which, in turn, explains the higher ARCs obtained for these reconstructions.

Author Contributions: Conceptualization, R.A. and J.S.; methodology, R.A. and V.A.; validation, J.S.; formal analysis, R.A.; investigation, R.A., V.A. and J.S.; writing—original draft, R.A.; writing—review and editing, R.A. and J.S.; supervision, J.S. All authors have read and agreed to the published version of the manuscript.

Funding: This research received no external funding.

Data Availability Statement: The data presented in this study are available on request from the corresponding author.

Conflicts of Interest: The authors declare no conflicts of interest.

Abbreviations

The following abbreviations are used in this manuscript:

^{166}Ho-RE	Radioembolization with holmium-166 microspheres
^{90}Y	Yttrium-90
ARC	Activity Recovery Coefficient
CF	Calibration Factor
CNR	Contrast-to-noise ratio
CV	Coefficient of variation
EANM	European Association of Nuclear Medicine
FWHM	Full Width at Half Maximum
MC	Monte Carlo
MELP	Medium Energy Low Penetration
OSEM	Ordered Subset Expectation Maximization
PVE	Partial Volume Effect
Q_H	Contrast Recovery Coefficient
SIRT	Selective Internal Radiation Therapy
SPECT/CT	Single-Photon Emission Computed Tomography/Computed Tomography
VOI	Volume Of Interest

References

1. Reinders, M.T.; Smits, M.L.; van Roekel, C.; Braat, A.J. Holmium-166 Microsphere Radioembolization of Hepatic Malignancies. *Semin. Nucl. Med.* **2019**, *49*, 237–243. [CrossRef] [PubMed]
2. Stella, M.; Braat, A.J.; Lam, M.G.; de Jong, H.W.; van Rooij, R. Gamma camera characterization at high holmium-166 activity in liver radioembolization. *EJNMMI Phys.* **2021**, *8*, 22. [CrossRef] [PubMed]
3. Stella, M.; Braat, A.J.; van Rooij, R.; de Jong, H.W.; Lam, M.G. Holmium-166 Radioembolization: Current Status and Future Prospective. *Cardiovasc. Interv. Radiol.* **2022**, *45*, 1634–1645. [CrossRef] [PubMed]
4. Smits, M.L.; Elschot, M.; Bosch, M.A.V.D.; Maat, G.H.V.D.; Schip, A.D.V.H.; Zonnenberg, B.A.; Seevinck, P.R.; Verkooijen, H.M.; Bakker, C.J.; Jong, H.W.D.; et al. In vivo dosimetry based on SPECT and MR imaging of ^{166}Ho-microspheres for treatment of liver malignancies. *J. Nucl. Med.* **2013**, *54*, 2093–2100. [CrossRef] [PubMed]
5. Wit, T.C.D.; Xiao, J.; Nijsen, J.F.W.; Schip, F.D.V.H.; Staelens, S.G.; Rijk, P.P.V.; Beekman, F.J. Hybrid scatter correction applied to quantitative holmium-166 SPECT. *Phys. Med. Biol.* **2006**, *51*, 4773–4787. [CrossRef]
6. Bonutti, F.; Avolio, M.; Magro, G.; Cecotti, A.; Schiava, E.D.; Do, E.D.; Longo, F.; Herassi, Y.; Bentayeb, F.; Rossi, M.; et al. Optimization of the image contrast in SPECT-CT bremsstrahlung imaging for Selective Internal Radiation Therapy of liver malignancies with Y-90 microspheres. *arXiv* **2015**, arXiv:1509.08857.
7. Salvat, F.; Fernández-Varea, J.M.; Baró, J.; Sempau, J. PENELOPE, an Algorithm and Computer Code for Monte Carlo Simulation of Electron-Photon Showers. 1996. Available online: https://www.osti.gov/etdeweb/servlets/purl/20930131 (accessed on 13 February 2024).

8. Porter, C.A.; Bradley, K.M.; Hippeläinen, E.T.; Walker, M.D.; McGowan, D.R. Phantom and clinical evaluation of the effect of full Monte Carlo collimator modelling in post-SIRT yttrium-90 Bremsstrahlung SPECT imaging. *EJNMMI Res.* **2018**, *8*, 7. [CrossRef] [PubMed]
9. Sjogreen-Gleisner, K.; Flux, G.; Bacher, K.; Chiesa, C.; de Nijs, R.; Kagadis, G.C.; Lima, T.; Georgosopoulou, M.L.; Gabina, P.M.; Nekolla, S.; et al. EFOMP policy statement NO. 19: Dosimetry in nuclear medicine therapy – Molecular radiotherapy. *Phys. Med.* **2023**, *116*, 103166. [CrossRef] [PubMed]
10. Danieli, R.; Milano, A.; Gallo, S.; Veronese, I.; Lascialfari, A.; Indovina, L.; Botta, F.; Ferrari, M.; Cicchetti, A.; Raspanti, D.; et al. Personalized Dosimetry in Targeted Radiation Therapy: A Look to Methods, Tools and Critical Aspects. *J. Pers. Med.* **2022**, *12*, 205. [CrossRef] [PubMed]
11. Ramonaheng, K.; van Staden, J.A.; du Raan, H. The effect of calibration factors and recovery coefficients on ^{177}Lu SPECT activity quantification accuracy: A Monte Carlo study. *EJNMMI Phys.* **2021**, *8*, 27. [CrossRef] [PubMed]
12. Peters, S.M.; van der Werf, N.R.; Segbers, M.; van Velden, F.H.; Wierts, R.; Blokland, K.J.A.; Konijnenberg, M.W.; Lazarenko, S.V.; Visser, E.P.; Gotthardt, M. Towards standardization of absolute SPECT/CT quantification: A multi-center and multi-vendor phantom study. *EJNMMI Phys.* **2019**, *6*, 29. [CrossRef]
13. Emission Computed Tomography (ECT) Phantoms. 2001. Available online: http://www.orion-france.com/pdf/catalogues/Orion_Data_Spectrum.pdf (accessed on 16 September 2023).
14. Elschot, M.; Vermolen, B.J.; Lam, M.G.; de Keizer, B.; van den Bosch, M.A.; de Jong, H.W. Quantitative Comparison of PET and Bremsstrahlung SPECT for Imaging the In Vivo Yttrium-90 Microsphere Distribution after Liver Radioembolization. *PLoS ONE* **2013**, *8*, e55742. [CrossRef]
15. Alqahtani, M.M.; Willowson, K.P.; Constable, C.; Fulton, R.; Kench, P.L. Optimization of ^{99m}Tc whole-body SPECT/CT image quality: A phantom study. *J. Appl. Clin. Med. Phys.* **2022**, *23*, e13528. [CrossRef] [PubMed]
16. Cherry, S.; Sorenson, J.; Phelps, M. *Physics in Nuclear Medicine*; Elsevier: Amsterdam, The Netherlands, 2012.
17. Gear, J.I.; Cox, M.G.; Gustafsson, J.; Gleisner, K.S.; Murray, I.; Glatting, G.; Konijnenberg, M.; Flux, G.D. EANM practical guidance on uncertainty analysis for molecular radiotherapy absorbed dose calculations. *Eur. J. Nucl. Med. Mol. Imaging* **2018**, *45*, 2456–2474. [CrossRef]
18. Morey, A.M.; Kadrmas, D.J. Effect of varying number of OSEM subsets on PET lesion detectability. *J. Nucl. Med. Technol.* **2013**, *41*, 268–273. [CrossRef]

Disclaimer/Publisher's Note: The statements, opinions and data contained in all publications are solely those of the individual author(s) and contributor(s) and not of MDPI and/or the editor(s). MDPI and/or the editor(s) disclaim responsibility for any injury to people or property resulting from any ideas, methods, instructions or products referred to in the content.